CONVERTING KNOWLEDGE INTO VALUE FOR OVER 30 YEARS

Since 1986

The study of residual thermal stresses on the performance of hybrid composite single lap joints

IAMaC2023

20/07/2023

V.D.C. Pires[1], R.J.C. Carbas[1,2], E.A.S. Marques[2], L.F.M. da Silva[2]

[1] Institute of Science and Innovation in Mechanical and Industrial Engineering (INEGI), Rua Dr. Roberto Frias, 4200-465 Porto, Portugal

[2] Department of Mechanical Engineering, Faculty of Engineering, University of Porto, Porto, Portugal

IAMaC2023

2nd Ibero-American Conference on Composite Materials

20th and 21th of July, 2023

driving science & innovation

Advanced Joining Processes Unit

CONTENT

1. Introduction

1.1. Background and motivation

1.2. The curved joint concept

1.3. Objectives

2. Experimental procedure

2.1. Materials

2.2. SLJ manufacturing

2.3. SLJ testing

3. Numerical details

3.1. Metal SLJ

3.2. Composite SLJ

4. Results

4.1. Metal SLJ

4.2. Composite SLJ

5. Conclusions

Since 1986

U.PORTO

1.

Introduction

- 1.1. Background and motivation
- 1.2. The curved joint concept
- 1.3. Objectives

Since 1986

1.1. Background and motivation

Composite materials in the aeronautical industry

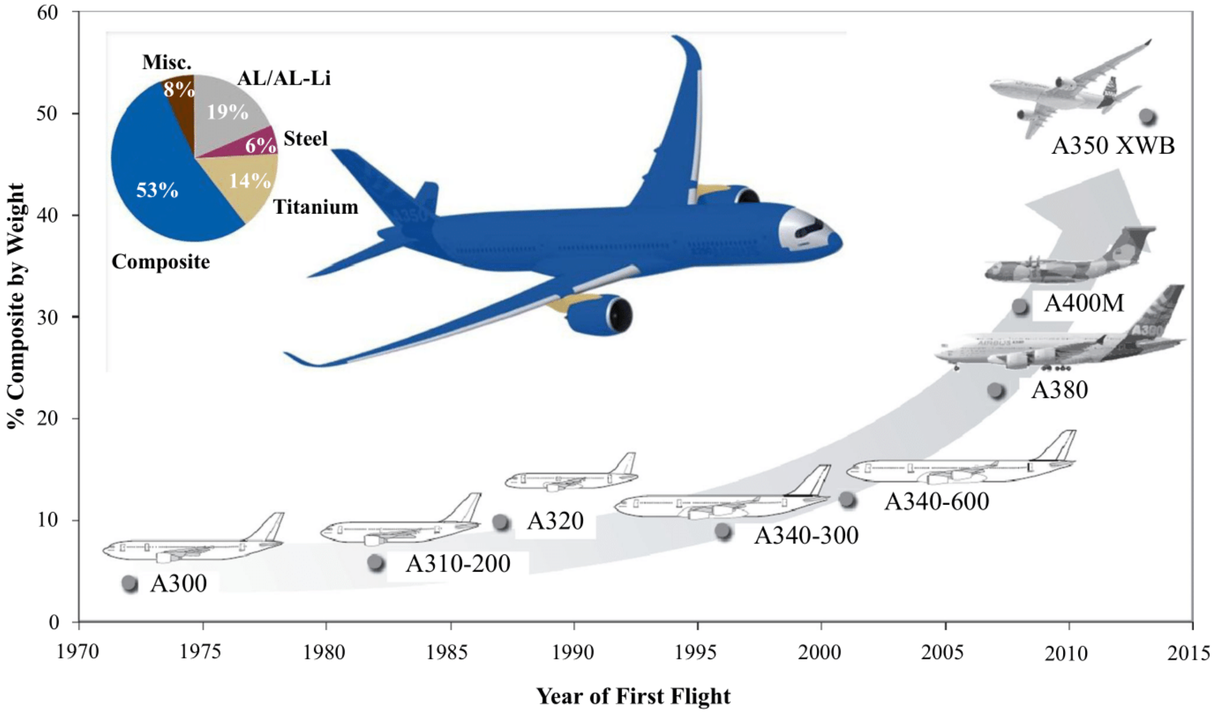

Figure 1 – Trends in the use of composite materials in commercial aircrafts [Xu et al., 2018].

1.1. Background and motivation

Regulatory hurdles regarding adhesive bounding

Non-destructive testing limitations and **delamination** caused are key barriers to the widespread adoption of adhesive bonding in aircraft structures.

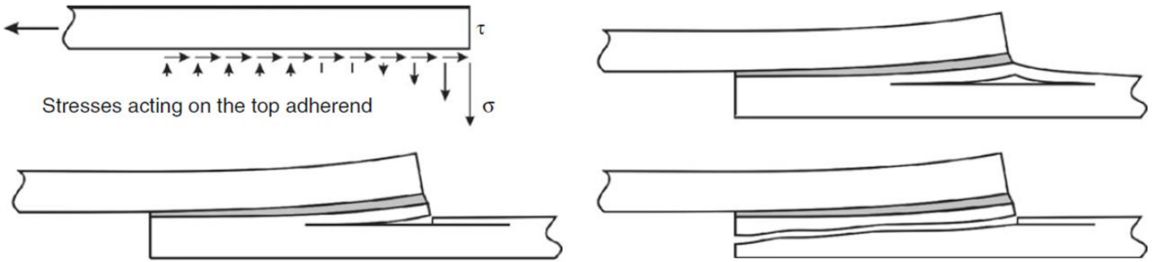

Figure 2 – Peel stress failure in adhesively bonded composite adherends [Hart Smith, 1973].

(a)

(b)

Figure 3 – Most prominent aviation regulatory bodies. (a) EASA in EU. (b) FAA in the US.

1.2. The curved joint concept

1 Introduction
Background and motivation
The curved joint concept
Objectives
2 Exp. procedure
3 Num. details
4 Results
5 Conclusions

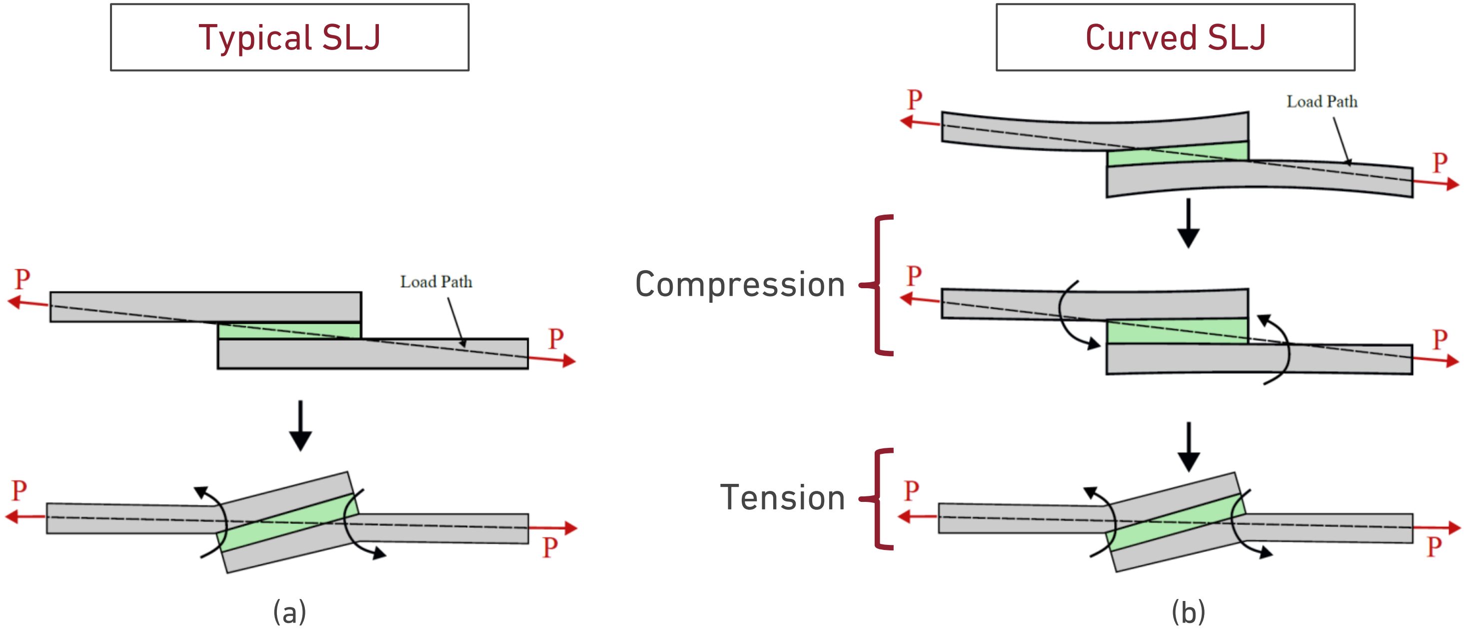

Figure 4 – Behaviour of SLJ under traction. (a) Planar SLJ. (b) Curved SLJ..

1.3. Objectives

Determination of material properties

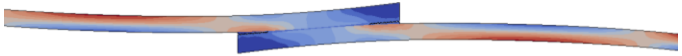

Numerical analysis

Experimental validation

Current study

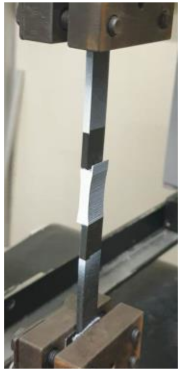

Real world applications

1 Introduction
Background and motivation
The curved joint concept
Objectives
2 Exp. procedure
3 Num. details
4 Results
5 Conclusions

2.

Experimental procedures

- 2.1. Materials
- 2.2. SLJ manufacturing
- 2.3. SLJ testing

inegi driving science & innovation

Advanced Joining Processes Unit

Since 1986

U.PORTO

2.1. Materials

Adhesive

3M Scotch AF163 2K

- Modified epoxy in film form;
- Aeronautical and aerospace applications.

1 Introduction
2 Exp. Procedure
Materials
SLJ manufacturing
SLJ testing
3 Num. Details
4 Results
5 Conclusions

Table 1 – AF 163-2K mechanical properties [dos Santos et al., 2019].

Young's modulus (GPa]	Tensile strength (MPa)	Shear modulus (MPa)	Shear strength (MPa)	G_{IC} (N/mm)	G_{IIC} (N/mm)	CTE $(\mu m/mK^{-1})$
1.521±0.118	46.9 ±0.6	159.73±41.9	46.9 ±2.57	4.05±0.07	9.77 ±0.21	90

2.1. Materials

Adherends

Table 2 – Orthotropic components for a unidirectional CFRP ply [Campilho et al., 2009].

Material	E_{11} [GPa]	E_{22} [GPa]	E_{33} [GPa]	v_{12} [-]	v_{13} [-]	v_{23} [-]	G_{12} [GPa]	G_{13} [GPa]	G_{23} [GPa]
CFRP	109	8.819	8.819	0.342	0.342	0.342	4.315	4.315	3.2

Table 3 – CFRP cohesive properties [Machado et al., 2017].

Material	t_n^0 [MPa]	t_s^0 [MPa]	G_{IC} [N/mm]	G_{IIC} [N/mm]
CFRP	109	8.819	8.819	0.342

Texipreg HS 160 REM

CFRP prepreg with ply thickness of 0.15mm.

Table 4 – CFRP CTE [Pereira et al., 2004].

Material	α_{11} [μm/mK^{-1}]	α_{22} [μm/mK^{-1}]	α_{22} [μm/mK^{-1}]
CFRP	-0.1	26	26

1 Introduction
2 Exp. Procedure
Materials
SLJ manufacturing
SLJ testing
3 Num. Details
4 Results
5 Conclusions

2.2. SLJ manufacturing

Adherends warping

Metal SLJ

Adherend curvature was obtained through mechanical **bending** and **plastic deformation**.

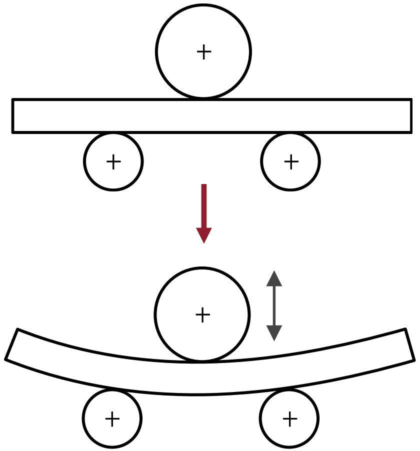

Previous study

Composite SLJ

Adherend curvature was obtained through **curing** of **asymmetric** composite layup.

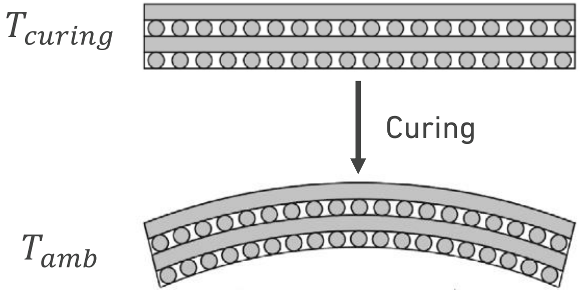

Current study

1 Introduction
2 Exp. Procedure
Materials
SLJ manufacturing
SLJ testing
3 Num. Details
4 Results
5 Conclusions

2.2. SLJ manufacturing

SLJ configurations and geometry

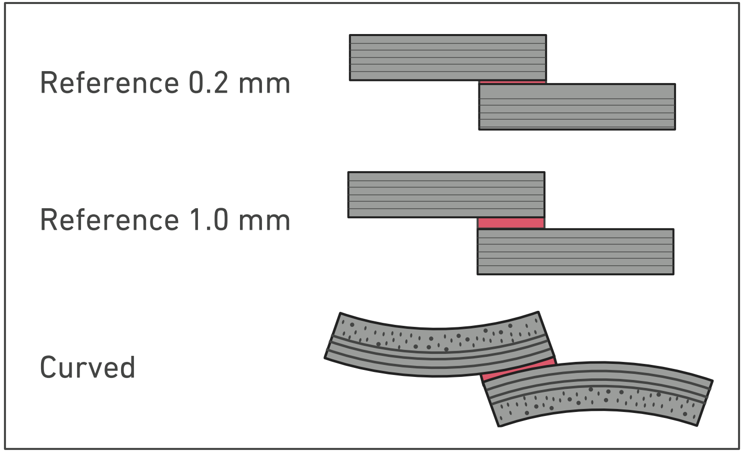

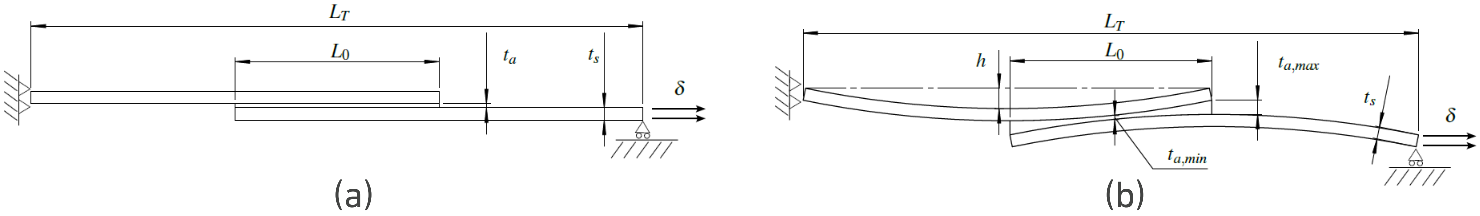

Figure 5 – SLJ specimen geometry. (a) Planar SLJ. (b) Curved SLJ.

2.3. SLJ testing

All tests were performed in an Instron® 3832 (Norwood, MA, USA) **quasi-static machine**.

Testing speed: 1mm/min

Standards followed:
1. ASTM D5868 (Composite SLJ)
2. ASTM D1002 (Metal SLJ)

Figure 6 – Experimental setup.

1 Introduction
2 Exp. Procedure
Materials
SLJ manufacturing
SLJ testing
3 Num. Details
4 Results
5 Conclusions

3.

Numerical details

- 3.1. Metal SLJ
- 3.2. Composite SLJ
- 3.3. Mesh and boundary conditions

Since 1986

3.1. Metal SLJ

Parametric elasto-plastic models

Nomenclature: $\Delta t_a\ X$, refers to the model with Xmm of extra maximum thickness relative to the reference

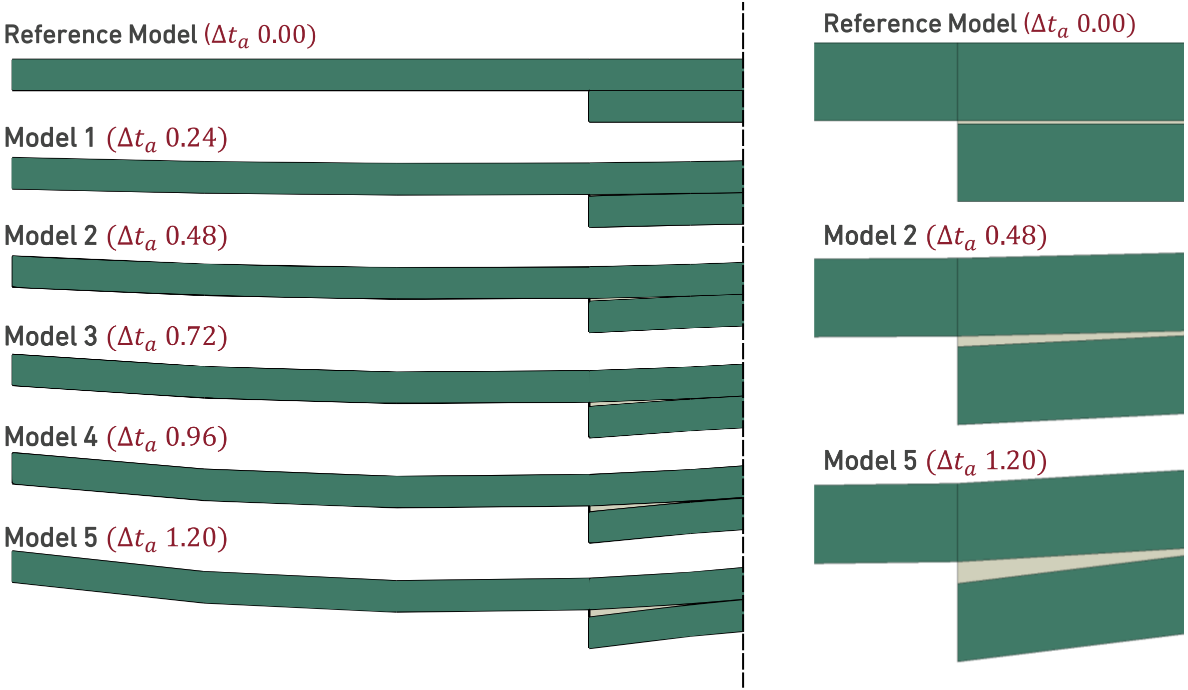

Previous study

Fig.7 – Parametric study with varying curvatures and maximum adhesive thicknesses. 2D static analysis in ABAQUS® software CPE4R elements (Plane Strain) were used for the elastic model

1 Introduction
2 Exp. Procedure
3 Num. Details
SLJ Designer app
Metal SLJ
Composite SLJ
Mesh and B.C
4 Results
5 Conclusions

3.3. Composite SLJ

CZM and XFEM models

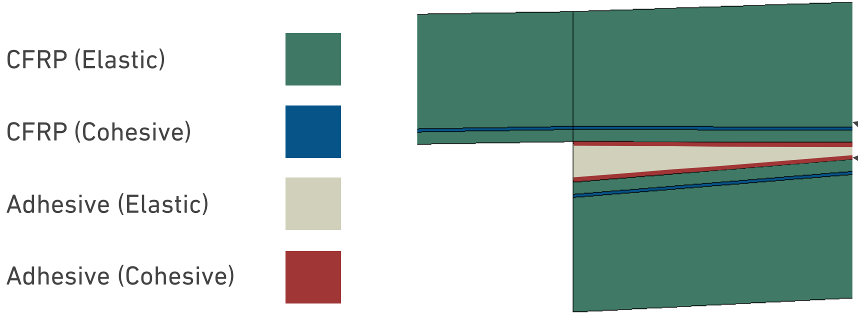

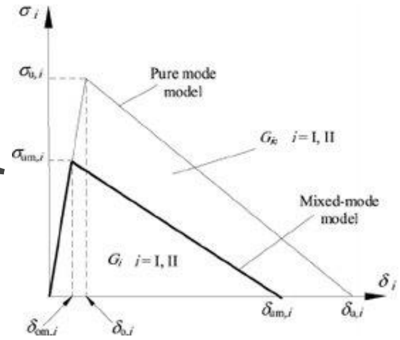

- 2D static analysis in ABAQUS® software
- **CPE4 elements** (Plane Strain) for the elastic sections
- **COH2D4 elements** (Cohesive) for the cohesive section

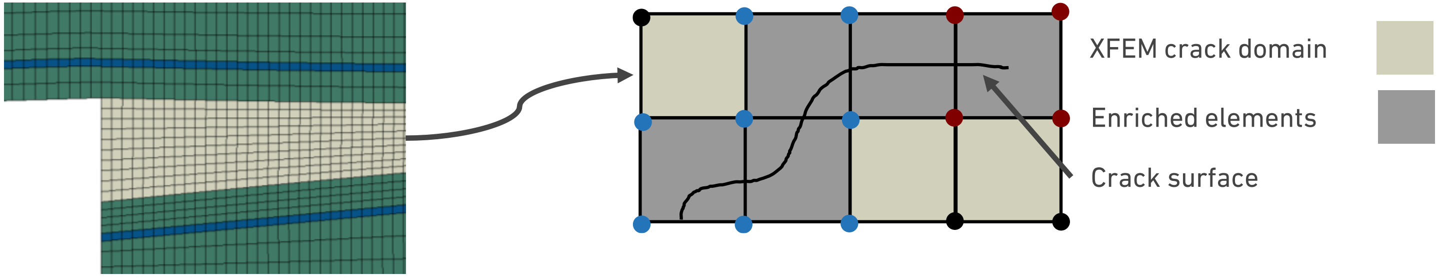

3.4. Mesh and boundary conditions

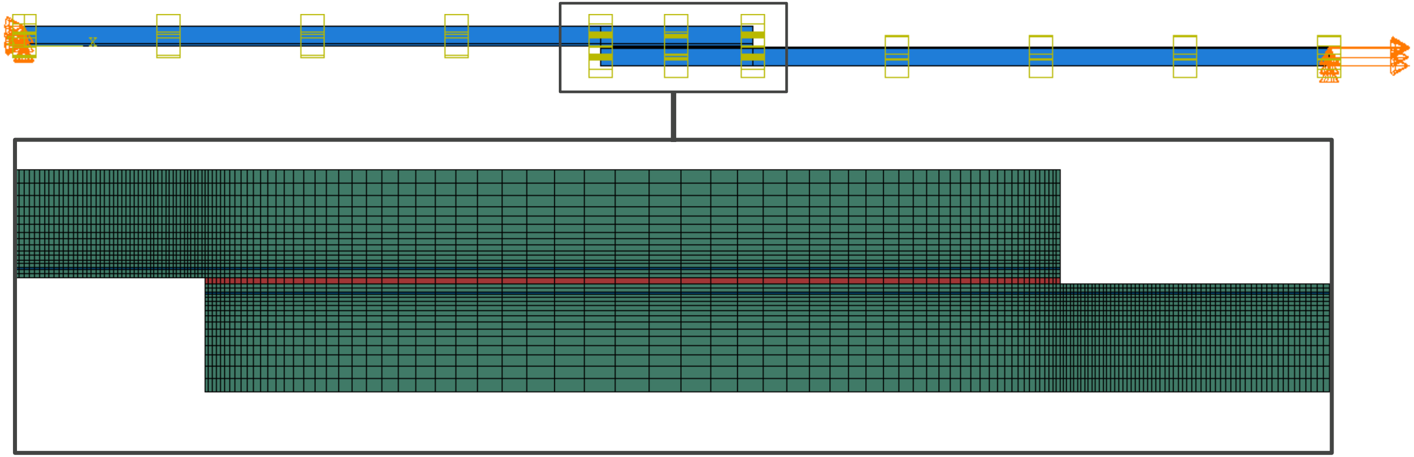

Fig.8 – Boundary conditions and mesh used for the SLJs numerical models.

- **ABAQUS Standard** is used for the quasi-static analysis
- **ABAQUS Explicit** used for the intermediate and impact analysis

Thermal step

- Initial T [°C]: 110
- Final T [°C]: 0

1 Introduction
2 Exp. Procedure
3 Num. Details
SLJ Designer app
Metal SLJ
Composite SLJ
Mesh and B.C
4 Results
5 Conclusions

4.

Results

- 4.1. Metal SLJ
- 4.2. Composite SLJ

Since 1986

4.1. Metal SLJ

Stress distributions

Previous study

1 Introduction

2 Exp. Procedure

3 Num. Details

4 Results

Metal SLJ

Composite SLJ

5 Conclusions

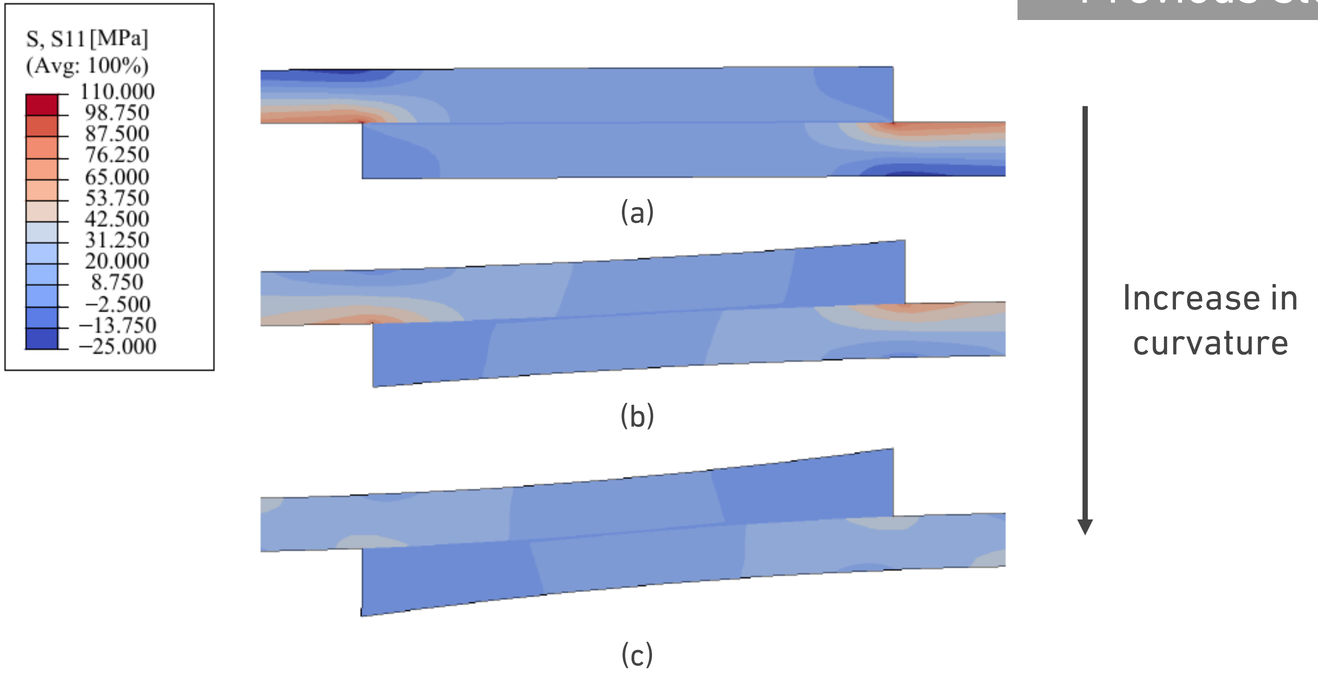

Fig.9 – Longitudinal stresses in MPa along the overlap length for the elastic models. (a) Reference. (b) Model 3. (c) Model 5.

4.1. Metal SLJ

Peel stress distributions

Previous study

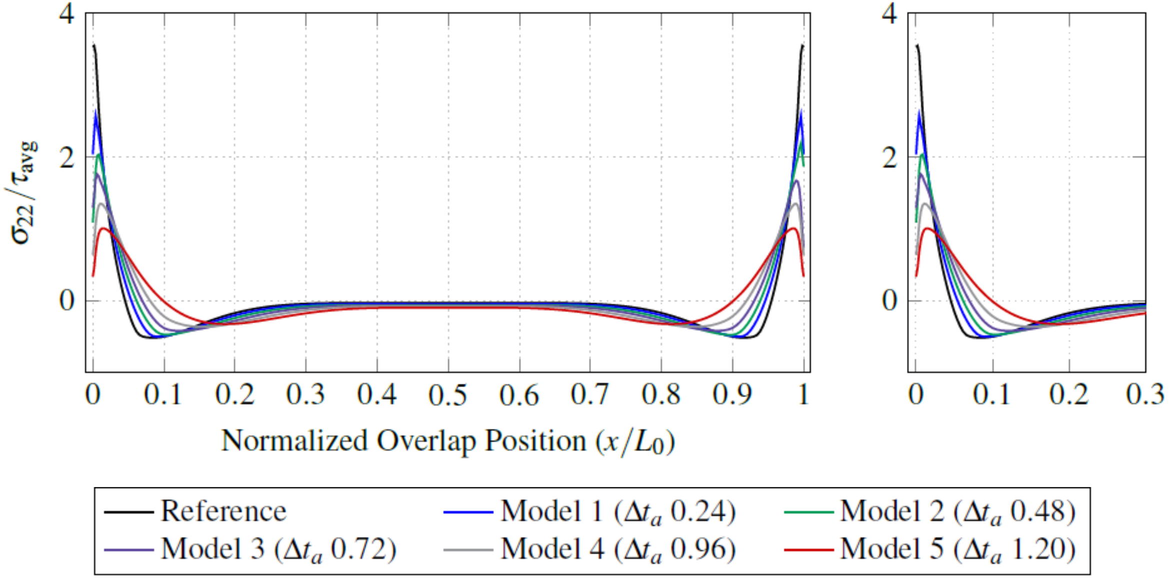

Fig.10 – Normalized peel stress distributions at the adhesive layer mid-thickness along the overlap.

1 Introduction
2 Exp. Procedure
3 Num. Details
4 Results
Metal SLJ
Composite SLJ
5 Conclusions

4.2. Composite SLJ

Peel stress distributions due to thermal stresses

Thermal effect only

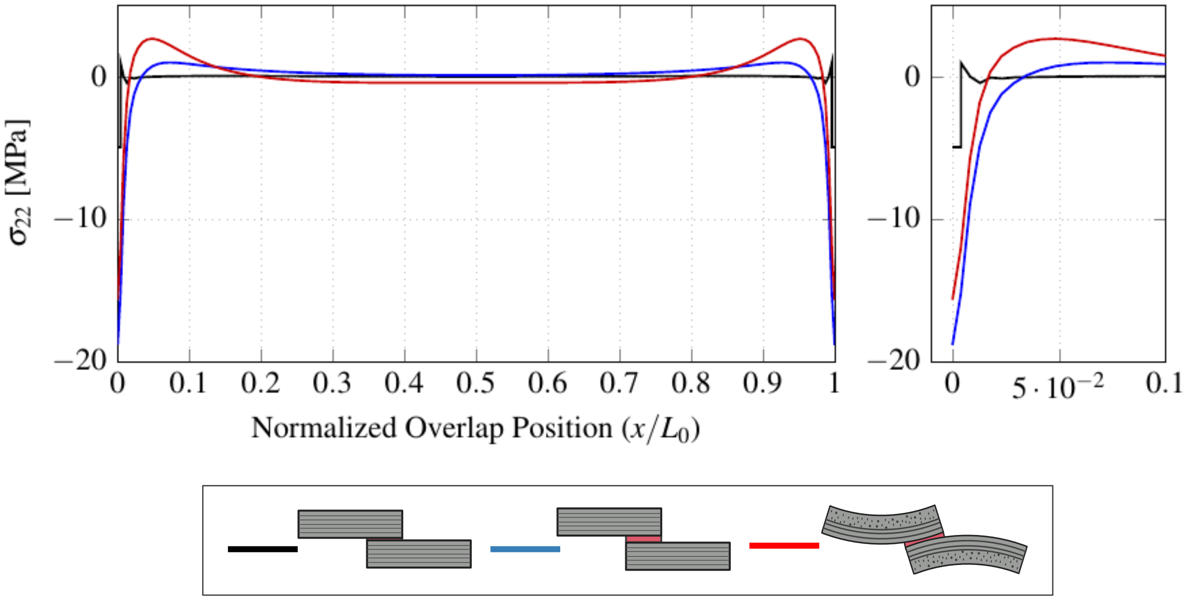

Fig.11 – Experimental and numerical failure mode for the studied SLJ. (a) Reference 0.2. (b) Reference 1.0mm. (c) Curved.

1 Introduction
2 Exp. Procedure
3 Num. Details
4 Results
Metal SLJ
Composite SLJ
5 Conclusions

4.2. Composite SLJ

Peel stress distributions after the mechanical step

Thermal + Mechanichal

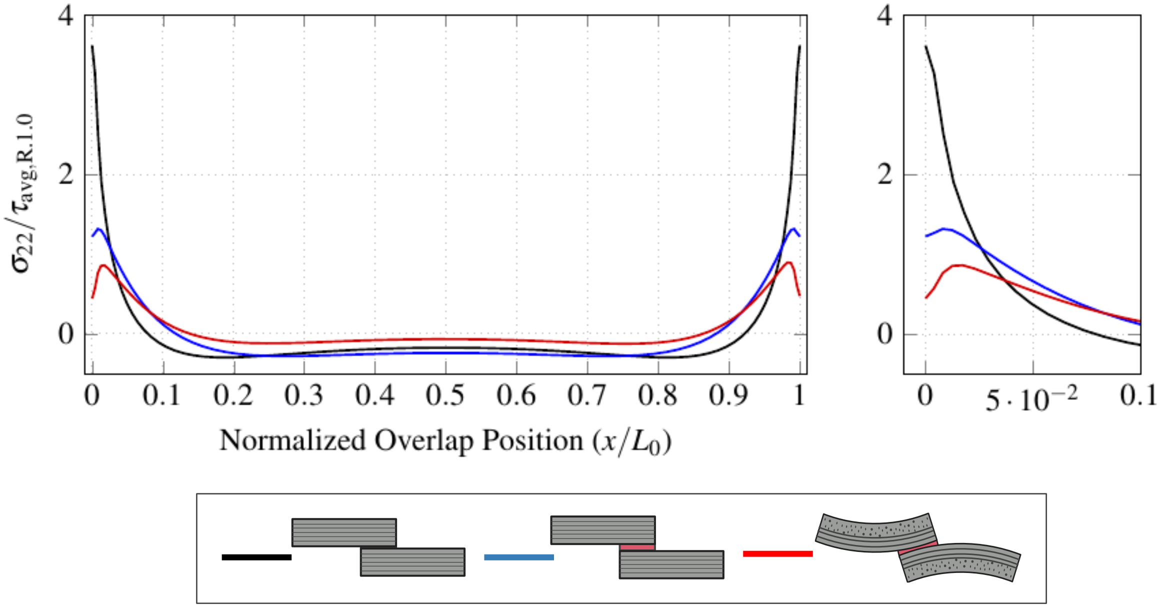

Fig.12 – Experimental and numerical failure mode for the studied SLJ. (a) Reference 0.2. (b) Reference 1.0mm. (c) Curved.

1 Introduction
2 Exp. Procedure
3 Num. Details
4 Results
Metal SLJ
Composite SLJ
5 Conclusions

4.2. Composite SLJ

Failure modes in quasi-static conditions

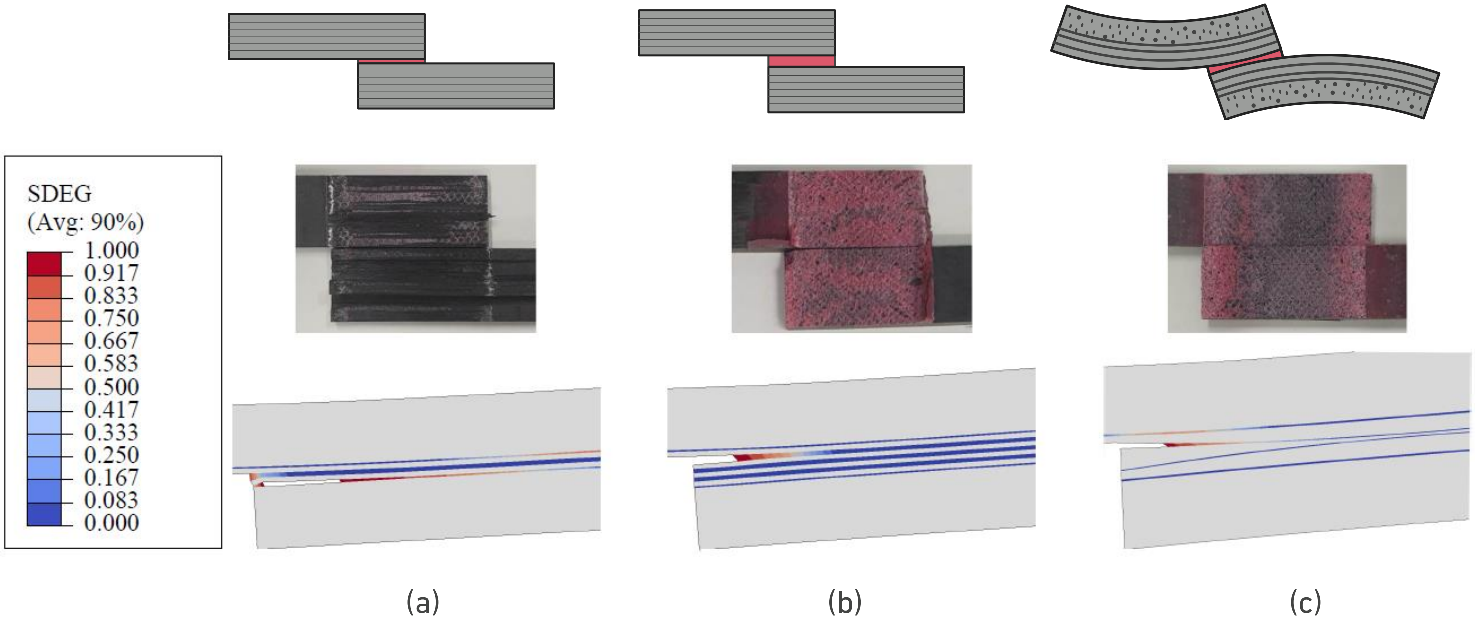

Fig.13 – Experimental and numerical failure mode for the studied SLJ.
(a) Reference 0.2. (b) Reference 1.0mm. (c) Curved.

1 Introduction
2 Exp. Procedure
3 Num. Details
4 Results
Metal SLJ
Composite SLJ
5 Conclusions

4.2. Composite SLJ

Joint performance in quasi-static

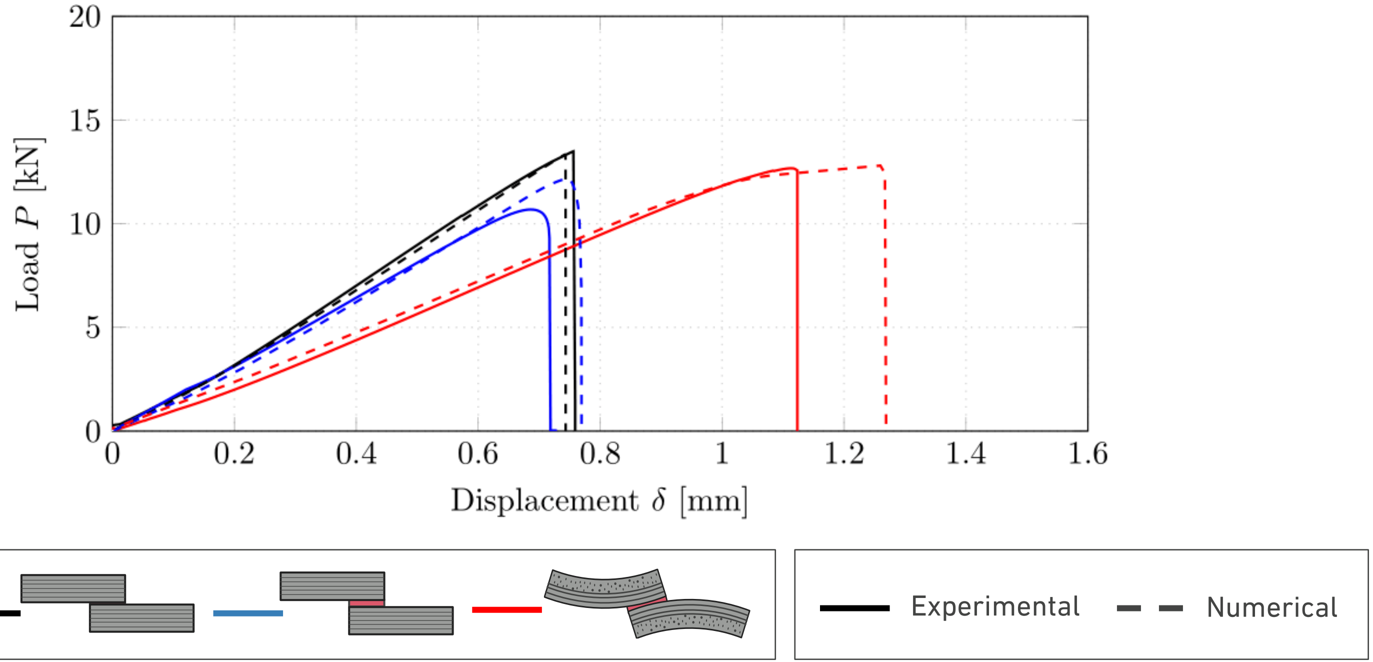

Fig.14 – $P - \delta$ curves obtained experimentally and numerical for all configurations.

4.2. Composite SLJ

Crack propagation

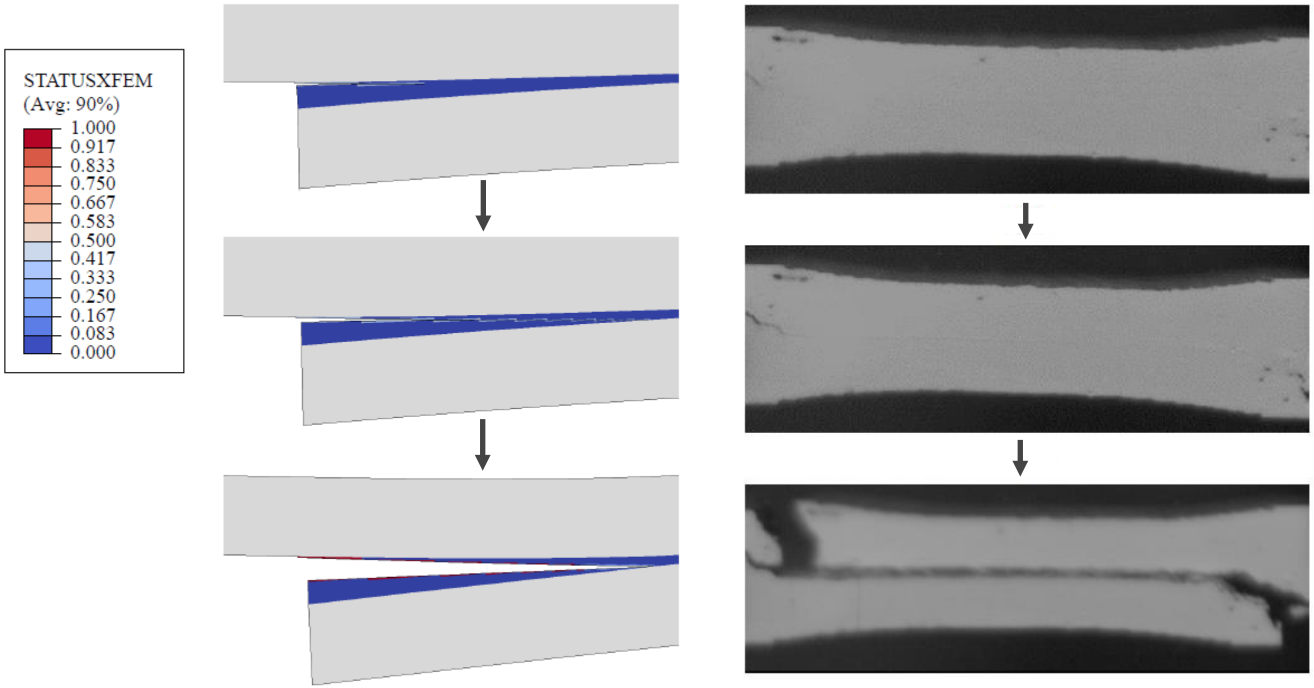

(a) (b)

Fig.15 – Crack propagation. (a) Numerical crack prediction. (b) Experimental crack propagation.

4.2. Composite SLJ

Crack propagation

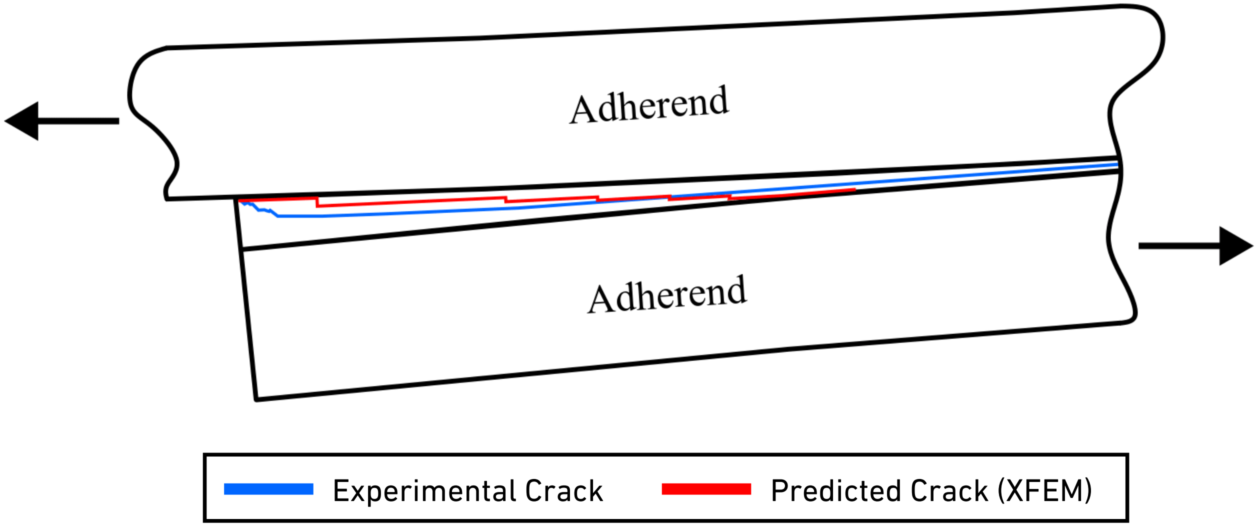

Fig.16 – Comparison between the numerical and experimental cracks.

4.2. Composite SLJ

Failure load for different strain rates

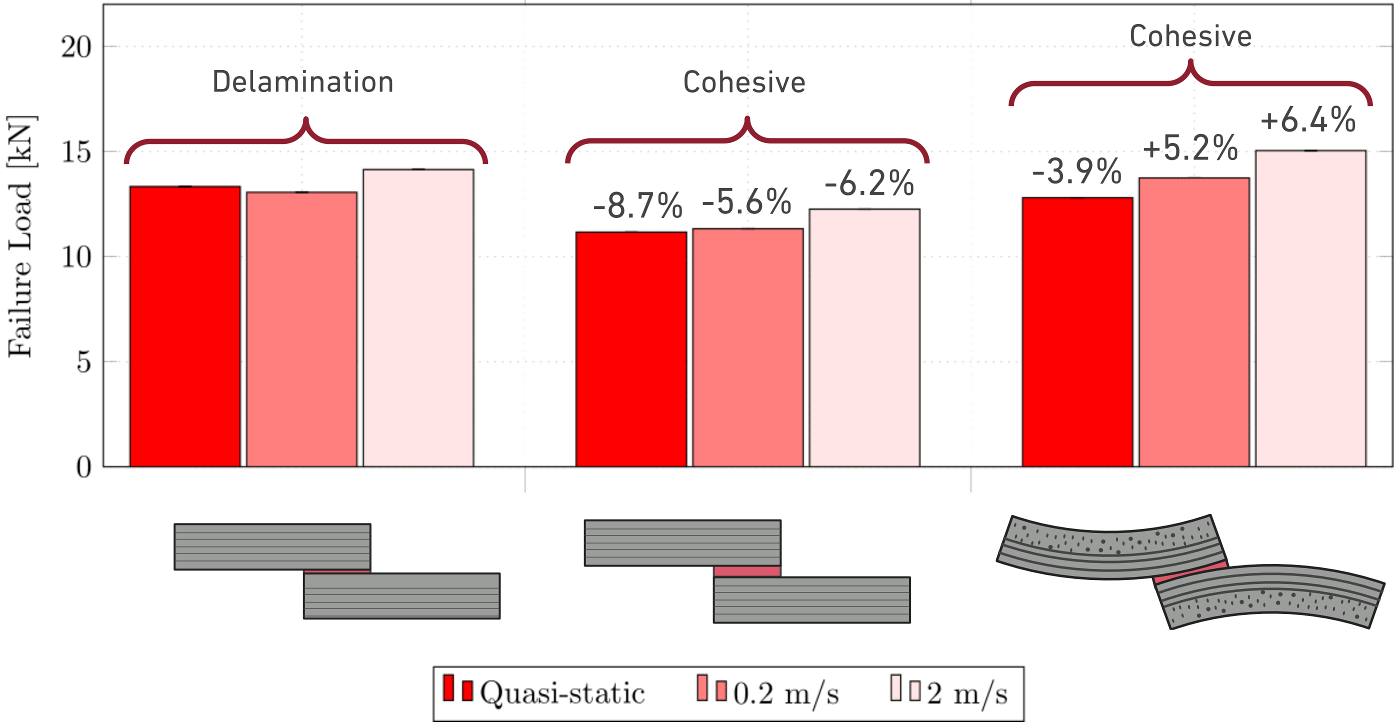

Fig.17 – Numerically predicted failure loads for each configuration for three different testing speeds..

1 Introduction
2 Exp. Procedure
3 Num. Details
4 Results
Metal SLJ
Composite SLJ
5 Conclusions

5.

Conclusions

driving science & innovation

Advanced Joining Processes Unit

Since 1986

U.PORTO

5. Conclusions

- This study showed that the use of the curved geometry significantly **decrease** the **peak stresses** in the overlap edges;

- Curved metal SLJs showed **increased energy absorption** with a ductile adhesive and significantly **improved failure load** when using with a brittle adhesive.

- The decrease of peak stresses, namely peel stresses on the overlap edges **prevented delamination**, allowing for a **cohesive** failure modes and improve performance on the composite SLJs.

- The curved composite SLJs successfully prevented delamination and exhibited higher failure loads, especially under **intermediate speed** and **impact conditions**. This can be attributed to their superior energy absorption capabilities observed in the study. These results emphasize the potential of curved SLJs as a reliable choice for various applications, including the aeronautical industry, where impact loadings are a significant concern.

driving science & innovation

ADVANCED JOINING PROCESSES UNIT

CONVERTING KNOWLEDGE INTO VALUE FOR OVER 30 YEARS

Since 1986

Thank you for your attention!

INSTITUTE OF SCIENCE AND INNOVATION IN MECHANICAL AND INDUSTRIAL ENGINEERING

www.inegi.up.pt

U.PORTO

6.

Backup Slides

Experimental details

Since 1986

Metal SLJ manufacturing

Manufacturing process flowchart

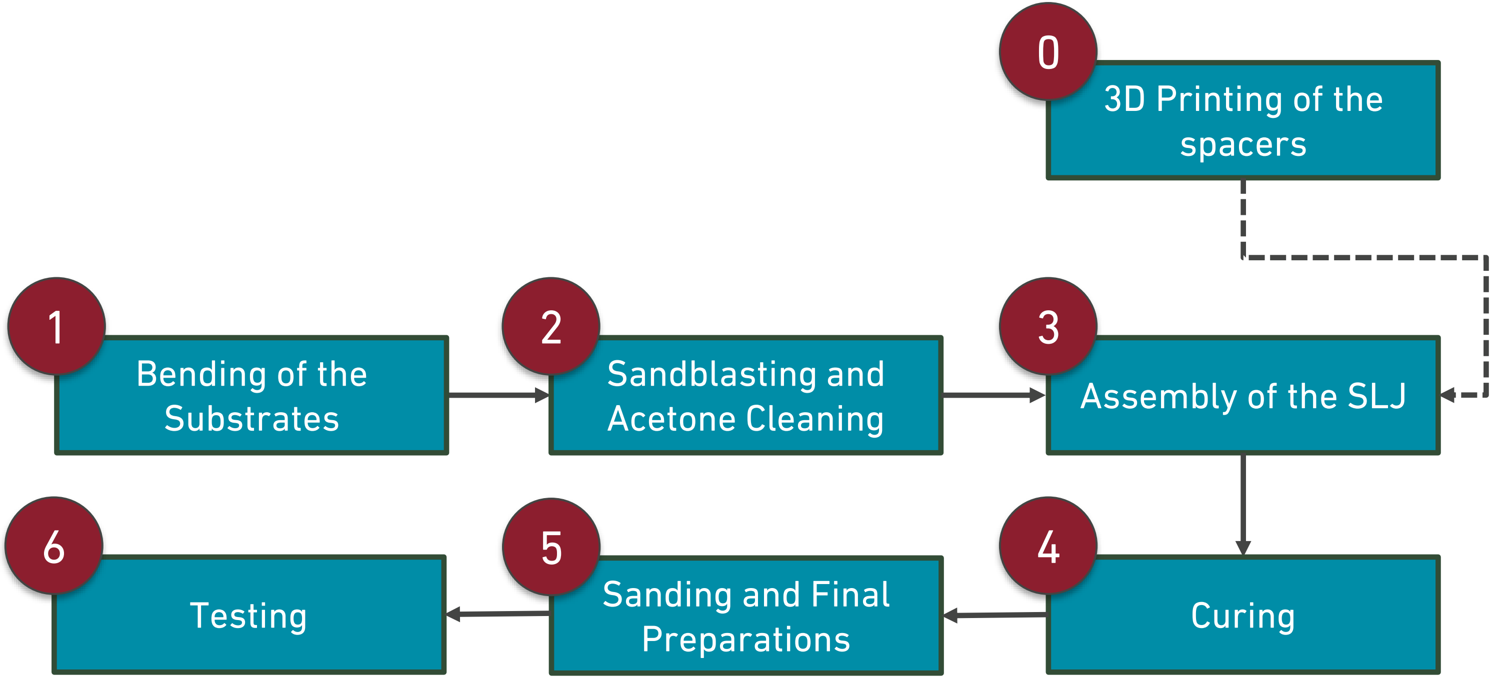

Metal SLJ manufacturing

Manufacturing details

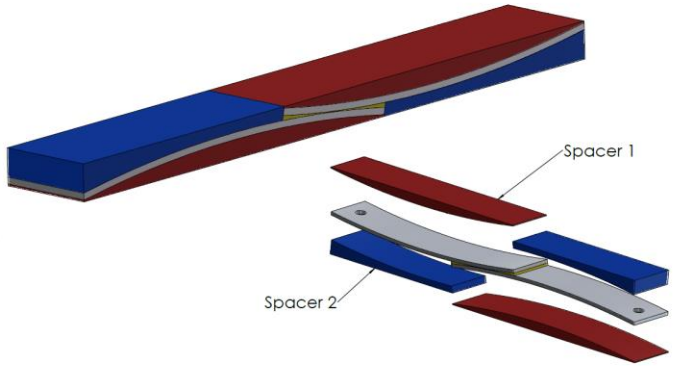

(a)

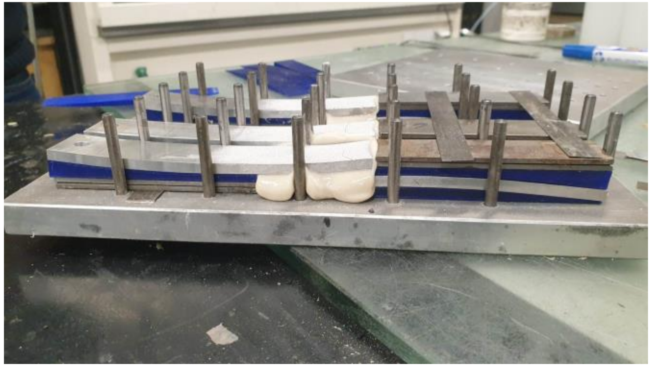

(b)

Figure 18 – (a) CAD of the SLJ. (b) Final assembly of the SLJs before curing.

Name	Type	Curing Conditions
2015-1	Ductile	8h @ T_{Room}
AV138	Brittle	24h @ T_{Room}

CFRP SLJ manufacturing

Manufacturing process flowchart

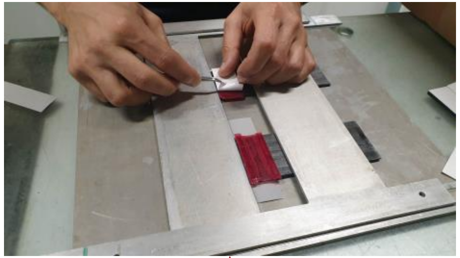

1. Hand layup of the CFRP prepreg plies
2. Adhesive stacking
3. Assembly in the mould
4. Co-Curing
5. Cutting Specimens

CFRP SLJ manufacturing

Co-curing mechanism (1 step)

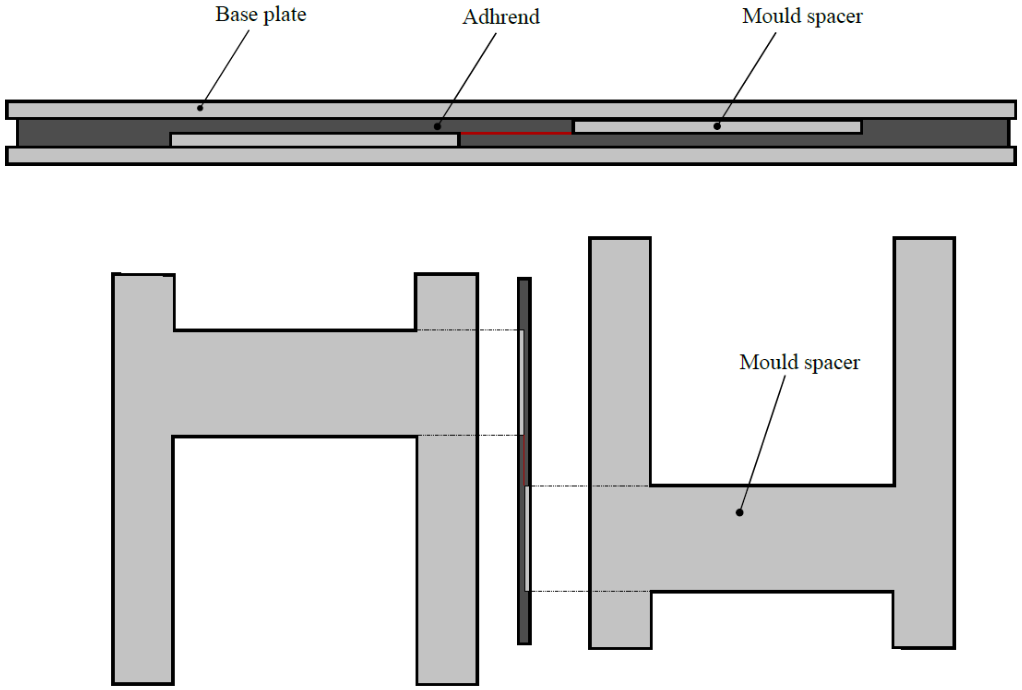

Fig.19 – Manufacturing mould scheme for co-curing.

CFRP SLJ manufacturing

Co-curing mechanism (1 step)

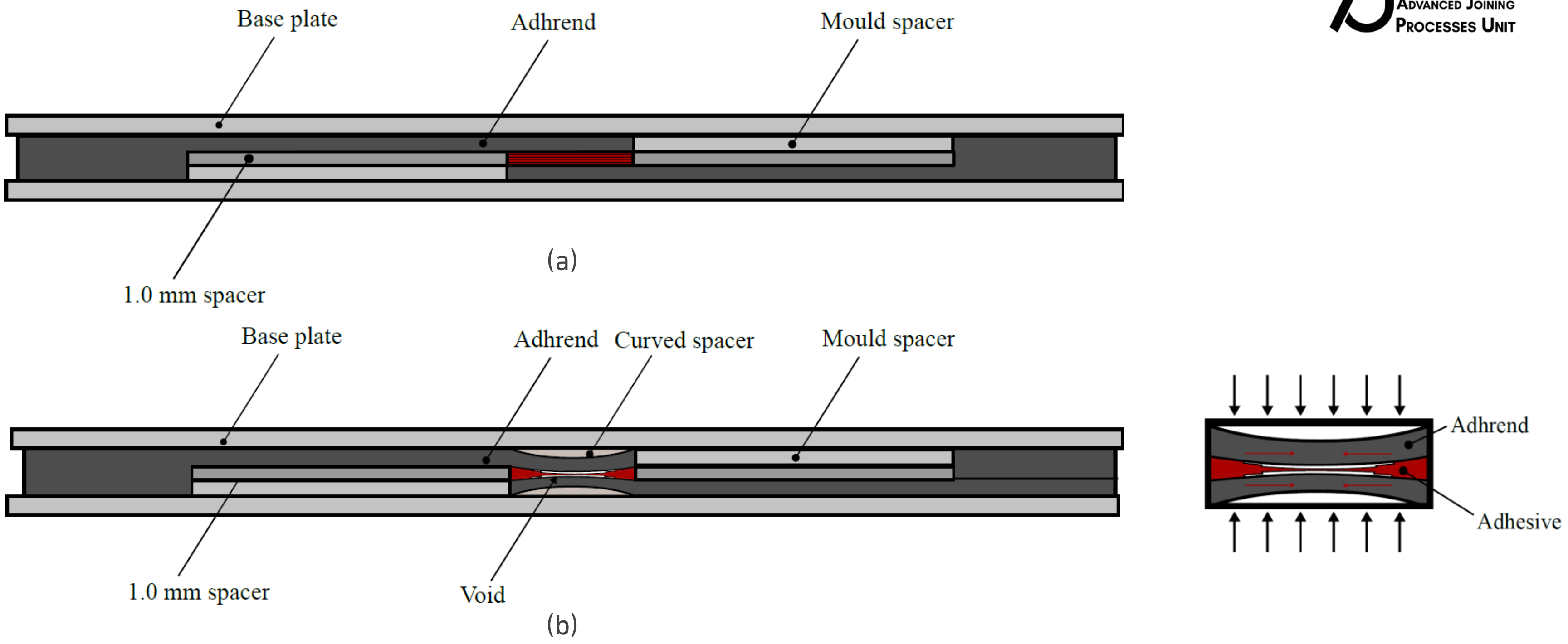

Fig.20 – Manufacturing mould scheme for co-curing of the (a) reference 1.0mm and (b) curved SLJs.

Surface treatments performed

Sandblasting

Phosphoric acid anodization (PAA)

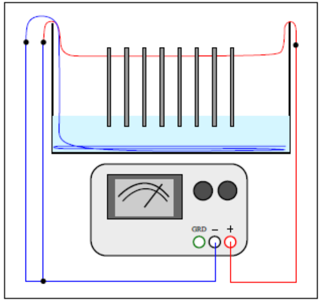

Atmospheric plasma treatment (APT)

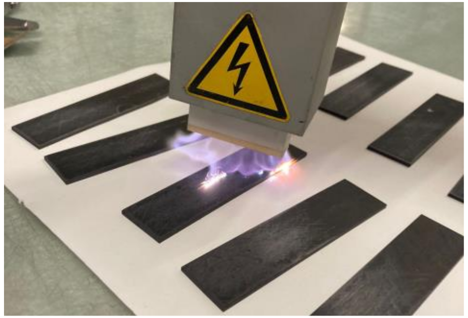

Warpage measurement of composite plates

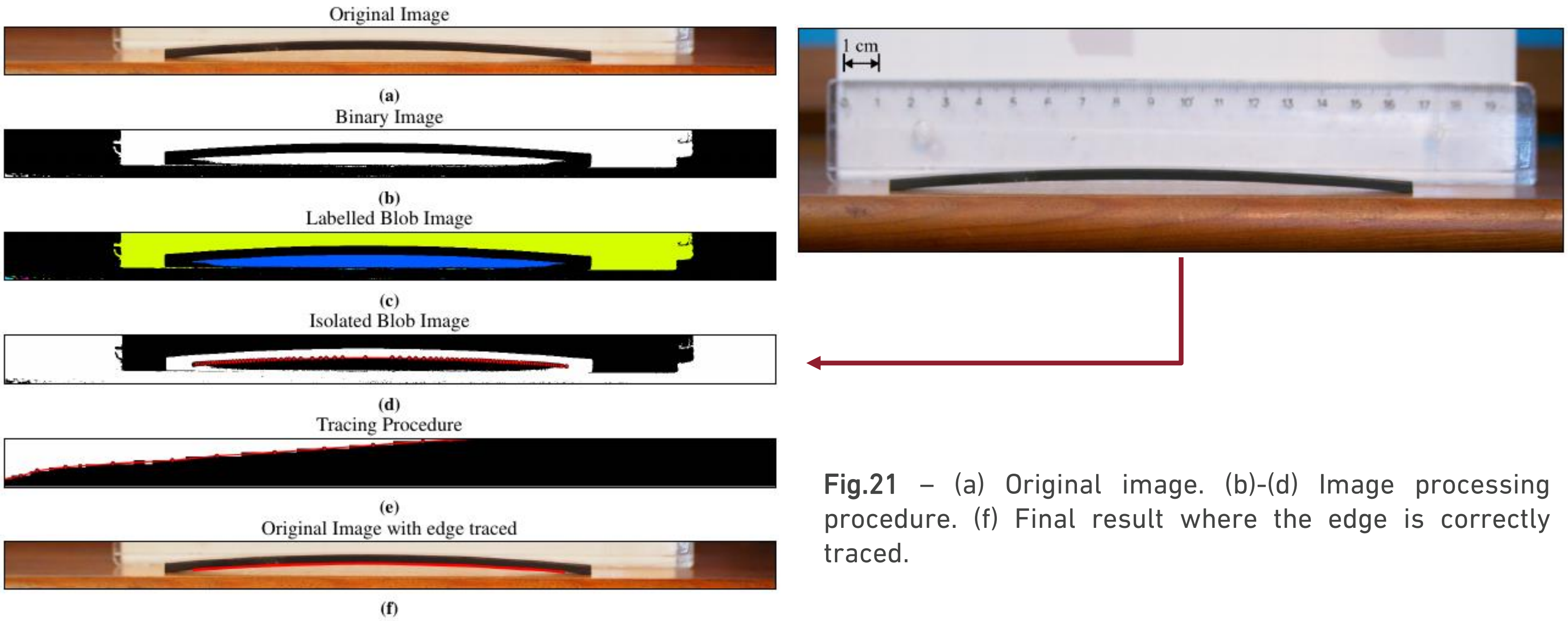

Fig.21 – (a) Original image. (b)-(d) Image processing procedure. (f) Final result where the edge is correctly traced.

7.

Backup Slides

Experimental details

Since 1986

Parameters and methods used for the numerical simulations

CZM models

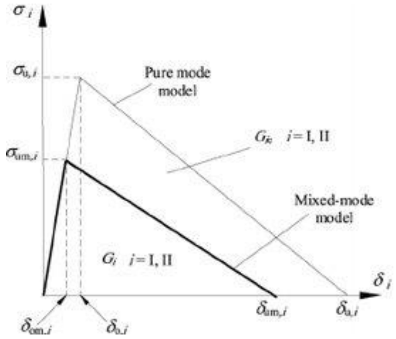

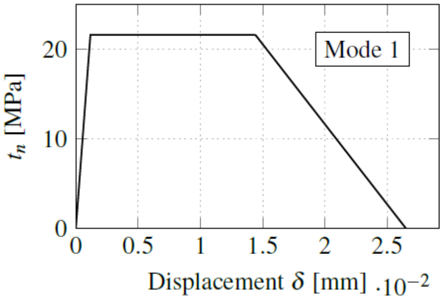

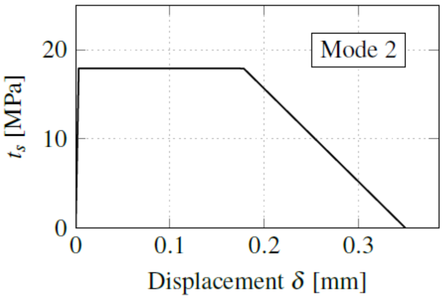

Trapezoidal CZM laws used in the modelling of Araldite®2015-1 for Mode 1 and Mode 2.

Damage initiation: QUADS

$$\left\{\frac{\langle t_n\rangle}{t_n^0}\right\}^2 + \left\{\frac{t_s}{t_s^0}\right\}^2 = 1$$

Mixed mode behaviour: Power law ($\beta = 1$)

$$\left\{\frac{G_n}{G_n^c}\right\}^\beta + \left\{\frac{G_{s1}}{G_s^c}\right\}^\beta = 1$$

Parameters and methods used for the numerical simulations

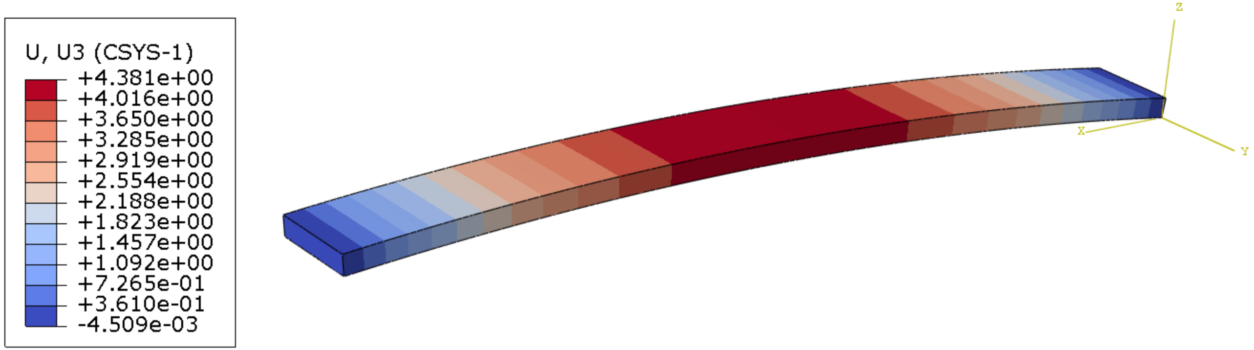

Fig.22 – Numerical simulation results of the composite warpage.

Table 5 – Numerical and experimental results of the observed maximum warpage of the asymmetric composite plates.

Layup	Numerical (mm)	Experimental (mm)	Error (%)
L5	3.49	3.51	0.76

Parameters and methods used for the numerical simulations

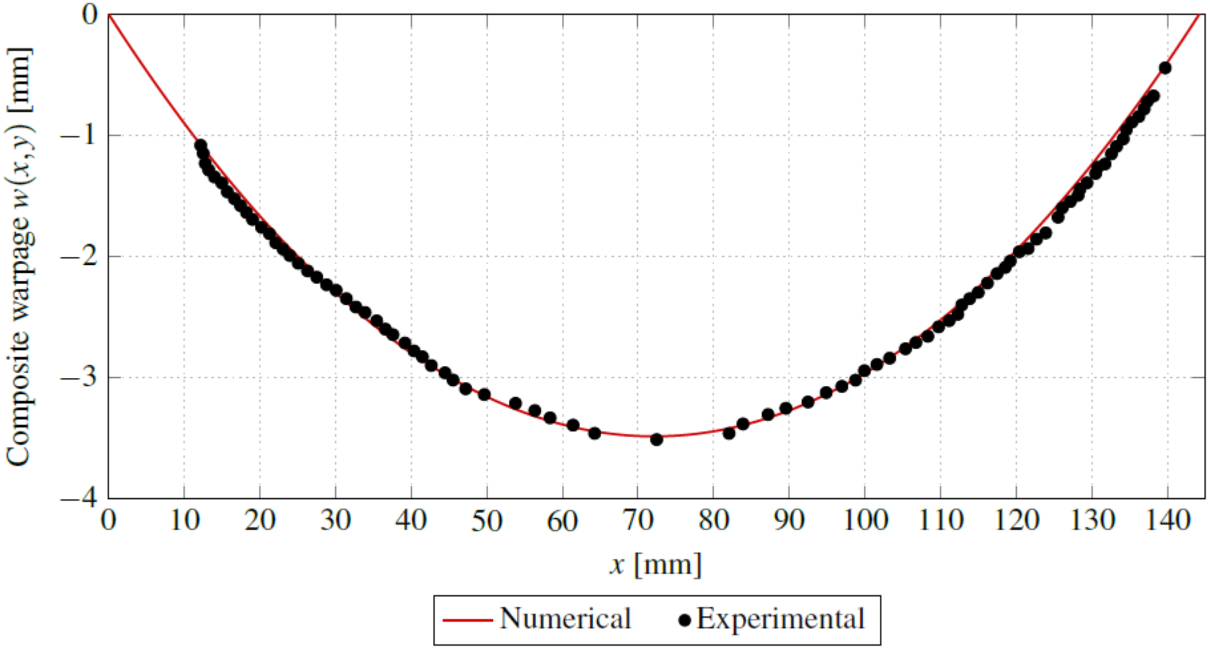

Fig.23 – Warpage of the composite adherend L5 due to thermal stresses.

8.

Backup Slides

Metal SLJ results

Since 1986

U.PORTO

Metal SLJ

Failure modes

2015-1 (Ductile) | AV138 (Brittle)

Reference

Curved

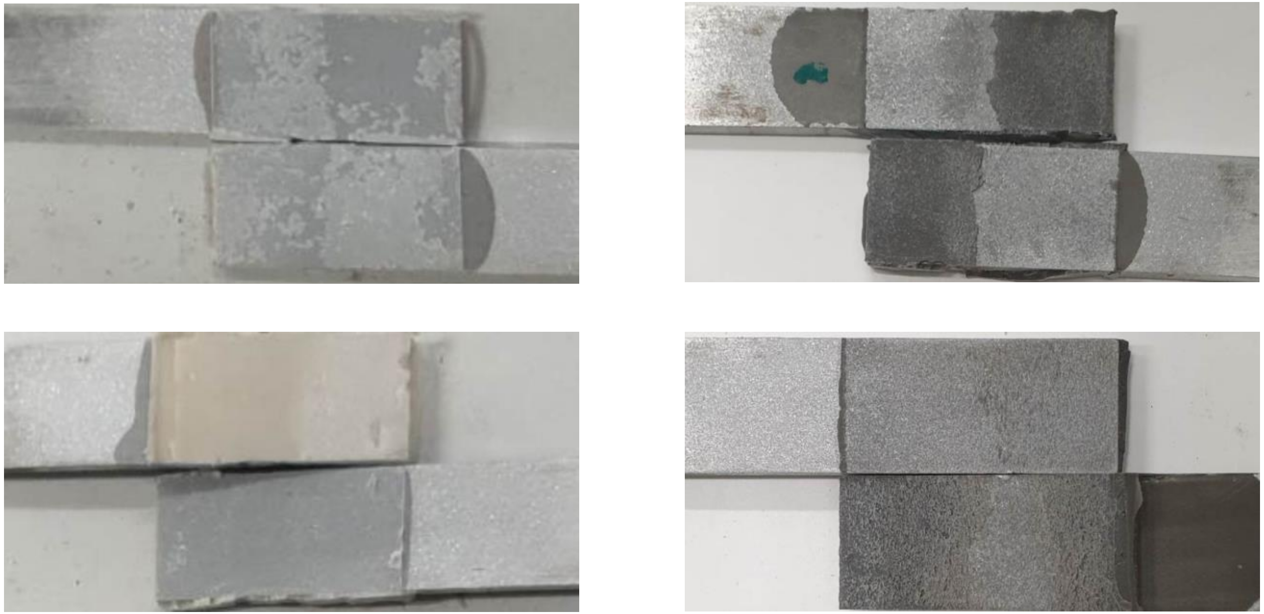

Fig.24 – Experimental failure mode for the reference and curved joints.

Metal SLJ

Joint performance

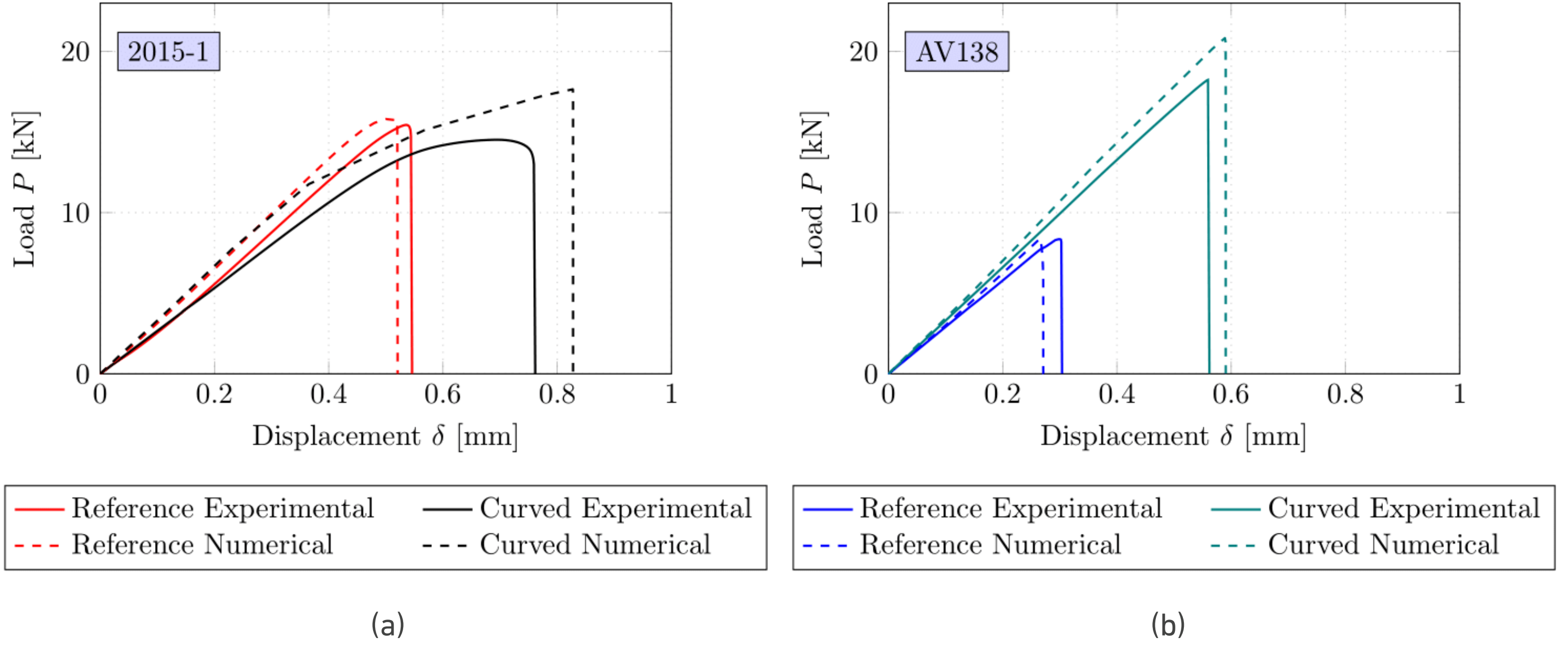

Fig.25 – $P - \delta$ curves obtained experimentally and numerical for both adhesives. The curved configuration corresponds to the geometry with the highest curvature. (a) 2015-1 (b) AV138.

Metal SLJ

Summary

- Curved SLJs with ductile adhesives didn't improve failure load but had a **62% increase in absorbed energy**.
- Curved SLJs with brittle adhesive showed a **131% increase in failure load** and a 291% increase in absorbed energy, due to **sensitivity to peak stresses** at overlap edges.

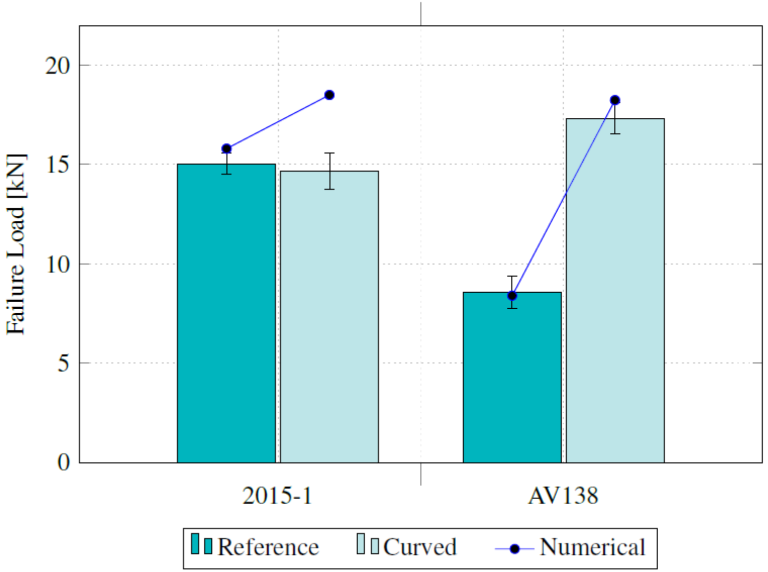

Fig.26 – Failure load for the reference and curved joints bonded with Araldite®2015-1 and AV138.